Using Tip Injection to Stability Enhancement of a Transonic Centrifugal Impeller with Inlet Distortion

Z. Jahani, H. Khaleghi[†] and S. Tabejamaat

Department of Aerospace Engineering, Amirkabir University of Technology, 15875-4413, Tehran, Iran

†*Corresponding Author Email: khaleghi@aut.ac.ir*

ABSTRACT

This paper aims to understand the effects of circumferential inlet distortion and tip injection on a transonic impeller performance and flow field. For distorted inflow, the impeller is subjected to a stationary 120-degrees circumferential total pressure distortion. Full annulus unsteady three-dimensional analysis has been used to study the inlet distortion and tip injection effects on the impeller performance, stability and flow field. The results show that the circumferential inlet distortion reduces the impeller total pressure ratio and adiabatic efficiency; however, it has no significant impact on the safe operating range. Unlike the inlet distortion, the tip injection considerably increases the operating range. According to the results, the distortion and tip injection effect on the compressor performance is mainly due to changes in tip leakage flow. The inlet distortion has unfavorable influences on the flow field, especially near the impeller tip; however, the tip injection ameliorates the flow field in this region. In both the clean and distorted inflow, the tip injection causes downstream shock transmission, weakening the shock-tip leakage interaction. Hence, stall inception is postponed, and the impeller stability is improved in the presence of the tip injection.

NOMENCLATURE

Dist	distorted inflow		**Subscripts**	
DP	Design Point			
Inj	tip injection		adb	adiabatic
LE	Leading-Edge		amb	ambient
NSP	Near the Stall Point		in	inlet
TE	Trailing-Edge		j	injection flow
y^+	non-dimensional wall distance		op	operating point
ω	rotation speed		out	outlet
			t	total

1. INTRODUCTION

Performance prediction is vital in centrifugal compressors due to their widespread industrial usage. Radial and circumferential inlet distortion may occur due to flow separation, growth of the boundary layer in the inlet duct and rotating stall occurring in the upstream stages. The inlet distortion often has unfavorable influences on compressor performance and stability. Flow non-uniformity at a compressor inlet influences the performance of all components located at the compressor downstream. Inlet flow distortion in aerial applications degrades the engine performance in terms of the thrust force and specific fuel consumption. It may also result in surge phenomena or engine flameout in critical conditions. Therefore, it is significantly required to model the flow through compressors in the presence of inlet distortion.

Some studies have been carried out on the artificially created distortion in a circumferential direction (Reid 1969; Ariga *et al*. 1983; Longley *et al*. 1996; Hah *et al*. 1998; Spakovszky *et al*. 1998; Zemp *et al*. 2010; Zhang and Hou 2017; Dong *et al*. 2018; Zhang and Zheng 2018).

The experimental results by Reid (1969) on an axial compressor revealed that the circumferential inlet distortion induces more loss in the near stall pressure ratio compared to the equivalent radial distortion. Ariga *et al*. (1983) experimentally investigated both circumferential and radial inlet distortion on a low-

speed centrifugal compressor. The results indicated that the inlet distortion leads to unfavorable influences on compressor performance and stability. They found that the compressor performance sensitivity to the radial inlet distortion is more than that observed in the circumferential inlet distortion. Zemp *et al.* (2010) presented the studies on the vibratory response and the associated problems, as well as the performance degradation caused by the inlet distortion on a single-stage, vane-less industrial centrifugal compressor. They found that the total pressure ratio is reduced by about 6% due to the inlet distortion.

Inlet flow non-uniformities may occur due to upstream components, as documented in (Kim *et al.* 2001; Engeda *et al.* 2003; Vagnoli and Verstraete 2015; Zhao *et al.* 2017; Grimaldi and Michelassi 2019).

Kim *et al.* (2001) experimentally investigated the distortion generated downstream of two different inlet configurations (straight and bent pipe) on a centrifugal compressor. The results indicated that a secondary flow is developed in the curved section of the bent pipe. Therefore the following compressor is subjected to distorted inflow. They found that the bent pipe produces more pressure loss compared to the straight pipe (with the equivalent mean line length).

According to the mentioned sources, inlet distortion has adverse effects on the compressor performance, but different methods can be used to compensate for it. Some approaches to compressor performance improvement have been proposed in some studies (Stein *et al.* 2000; Suder *et al.* 2000; Iyengar *et al.* 2005; Beheshti *et al.* 2006; Khaleghi *et al.* 2008a; Hirano *et al.* 2012; Ma and Kim 2017; Yang *et al.* 2017; Dong *et al.* 2018; Taghavi-Zenouz and Behbahani 2018; Sun *et al.* 2019; Li *et al.* 2020; Li *et al.* 2021; Wang *et al.* 2021).

Tip injection is a beneficial approach to improve compressor performance and stability. The beneficial effects of tip injection on compressor performance, as well as the effects of different parameters (injector width, yaw, injection angle, or injector boundary conditions), have been investigated in some studies (Beheshti *et al.* 2006; Khaleghi *et al.* 2008b; Taghavi-Zenouz and Behbahani 2018).

A numerical analysis of the tip injection role on a low-speed centrifugal compressor performance was investigated by Stein *et al.* (2000). Their results demonstrated that by using an injected mass flow equivalent to 5 and 10 percent of the total mass flow rate, the compressor stable operating range is enhanced by about 47 and 65 percent, respectively. Discrete tip injection effects on a transonic compressor rotor were studied experimentally and numerically by Suder *et al.* (2000). The simulation results indicated that the tip injection suppresses the compressor instability by reducing the incidence angle and blade loading near the tip. Taghavi-Zenouz and Behbahani (2018) demonstrated that a small amount of injected mass (0.5% of the whole annulus

mass flow rate) causes an increment of 15.5% in the stall margin of a low-speed axial compressor rotor.

Although many studies have been done on inlet distortion or performance improvement methods, the mechanism of each in changing the performance or the simultaneous impact is still controversial, especially for radial compressors. This paper aims to fill the mentioned research gap. The impeller of SRV2-O was chosen as the test case. Unsteady three-dimensional computational fluid dynamics (CFD) code has been employed to solve the compressible Navier–Stokes equations.

2. TEST CASE

The numerical simulations have been performed on an impeller of a transonic centrifugal compressor, the so-called SRV2-O.

This compressor was designed and built at DLR. The impeller is unshrouded and has 13 main and 13 splitter blades. 3-D model and meridional view are shown in Figs. 1(a) and 1(b), respectively.

(a)   3D sketch

(b)   Meridional view
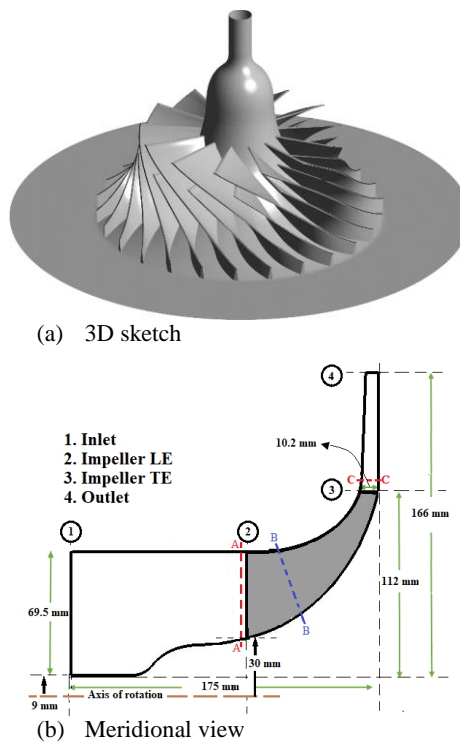
Fig. 1. Impeller Geometry.

Sections 1-4 shown in Fig. 1(b) correspond to the inlet, impeller LE, impeller TE, and outlet, respectively. Furthermore, sections A-A and C-C specified in this figure located just upstream of the impeller LE and downstream of the TE, respectively. Section B-B is defined at 25 percent of the impeller mean-line length upstream of the impeller LE. These sections will be used for validation and interpreting the results.

At the design point, the impeller tip clearance varies from 0.5 mm at the LE to 0.3 mm at the TE. The main

design specifications of SRV2-O are presented in Table 1.

Table 1 SRV2-O design specifications (Hah and Krain 1999)

Parameter	Value	Unit
Inlet Total Pressure	101325	Pa
Inlet Total Temperature	288.15	K
Rotational Speed	50000	RPM
Blade Count Full/Splitter	13/13	-
Impeller LE Root Radius	30	mm
Impeller LE Tip Radius	78	mm
Impeller TE Radius	112	mm
Impeller TE Blade Width	10.2	mm
Impeller LE Blade Angle at Tip	26.5	Degree
Impeller TE Blade Angle	52	Degree
Outlet Radius	175	mm
Nominal Tip Clearance	0.5 at LE / 0.3 at TE	mm

In order to tip injection study, a casing-mounted annular injection is applied in a region with 10 mm in width, at zero yaw angle, and 5-degree injection angle. The distance from the injector to the impeller LE at the tip is about 15 mm (35% of the main blade height at the LE). The injector configuration is shown in Fig. 2.
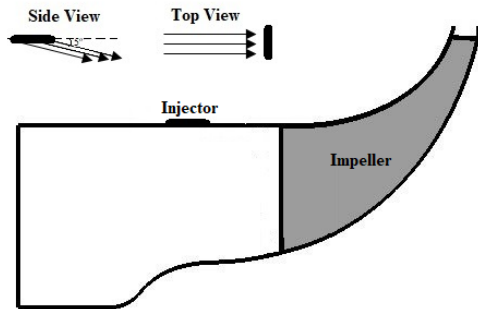
Fig. 2. Injector location.

3. NUMERICAL METHOD

A commercial CFD solver (CFX) was employed to solve the three-dimensional equations. Fifty time steps were set per blade passing period. The time step used is 3.7×10^{-6} s. The turbulence model was chosen to be SST. In the current study, the following boundary conditions were assigned:

Uniform total pressure, total temperature, and flow angles were specified at the inlet of the domain (section 1). Uniform static pressure was applied at the impeller outlet (section 4). The walls were considered to have nonslip and adiabatic conditions.

The non-uniform distribution of total pressure shown in Fig. 3 was used as the inlet boundary condition for the distorted inflow. The total pressure in this figure is normalized with the mass flow averaged and time-averaged total pressure at the inlet of the distorted inflow case. Other boundary conditions have been chosen to be the same as the clean inflow.

The total temperature and flow direction (zero yaw angle and 5-degree injection angle) were applied for the injector boundary conditions. The injector total pressure was set so that the injector exit Mach number became 0.8.
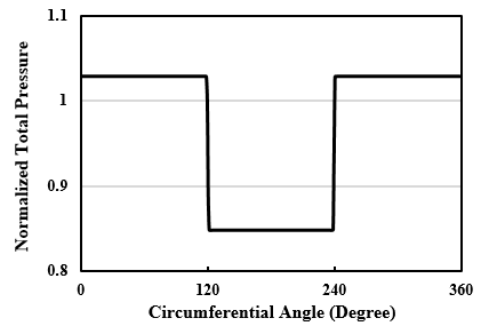
Fig. 3. Circumferential distribution of the normalized total pressure at the inlet of distorted inflow.

4. GRID INDEPENDENCY

The impeller grid was created in TurboGrid using a multi-block structure. Automatic topology (ATM) technique is used. The grid is clustered near the solid walls to meet the resolution requirements of y+ about one.

To verify the grid accuracy, steady simulations have been conducted for different grid sizes. Fig. 4. shows the design total pressure ratio and adiabatic efficiency for different grids. Grid independency analysis, as shown in this figure, proves that about 1.2 million nodes for a single passage are adequate to achieve acceptable results.
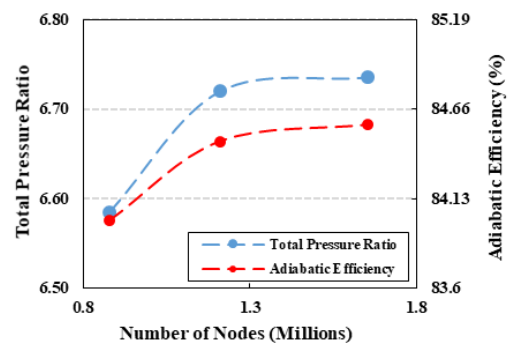
Fig. 4. Grid independency study.

To study the circumferential distortion, a full-annulus computation model is essential. So, the computational grid shown in Fig. 5, consisting of about 15.6 million nodes, was used.

5. VALIDATION

The experimental data presented in (Eisenlohr *et al.*, 1998; Eisenlohr *et al.*, 2002) have been used to validate the numerical results for the clean inflow with smooth casing. Fig. shows a comparison of
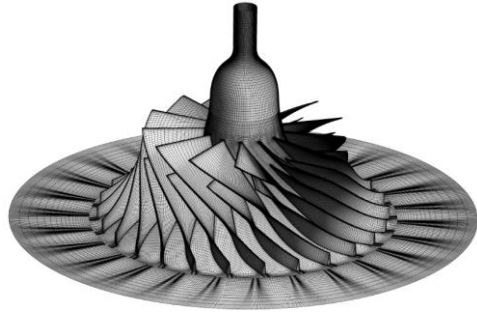
Fig. 5. Computational grid.

the impeller total pressure ratio and adiabatic efficiency resulting from the simulations at the design rotational speed (50000 rpm) and the experimental results presented by Eisenlohr *et al.* (2002). The design and near stall points are shown on Fig. 6(a) with DP and NSP, respectively. The design point is equivalent to a normalized mass flow of 0.89, and the near stall point was determined to be the last point before the divergence of the solution. The solution's convergence was monitored by tracking the outlet mass flow rate. The simulation was assumed as converged when the outlet mass flow rate variations with time became approximately zero. The mass flow rate is normalized by using the respective choking mass flow rate. The impeller total pressure ratio and adiabatic efficiency have been calculated based on the mass flow averaged parameters in sections A-A and C-C.
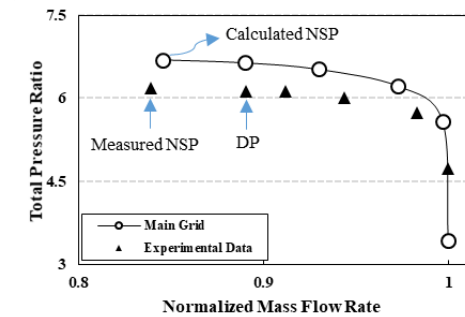
(a)   Total pressure ratio
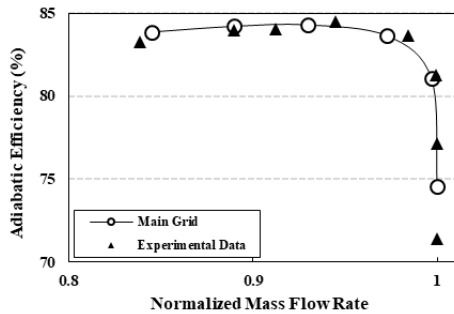
(b)   Adiabatic efficiency

Fig. 6. Performance curves for the clean inflow with smooth casing.

As Fig. 6 shows, the calculated adiabatic efficiency is in good agreement with experimental data.

However, the impeller total pressure ratio resulting from the simulations is slightly overestimated.

Figures 7 and 8 compare the experimental and numerical contours of the relative Mach number in sections A-A and 3, respectively (m_{op}/m_{choked} = 0.89).

(a)   Present work

(b)   Experiment data (Eisenlohr *et al.* 1998)
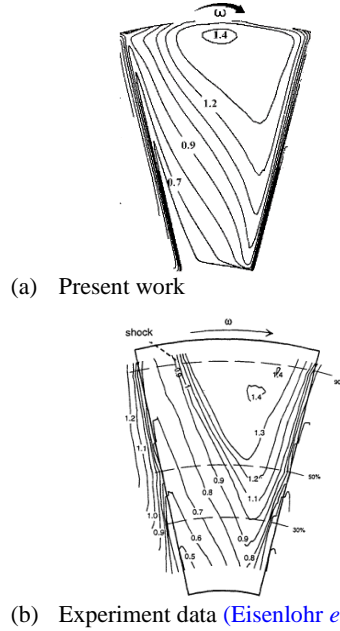
Fig. 7. Relative Mach number contours in section A-A and at the design point.

(a)   Present work

(b)   Experiment data (Eisenlohr *et al.* 2002)
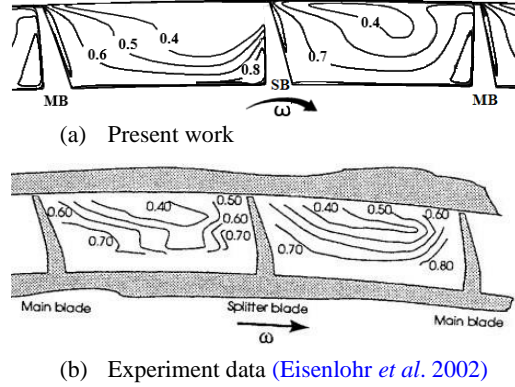
Fig. 8. Relative Mach number contours in section 3 and at the design point.

These figures show that the numerical results and the experimental data are in reasonable agreement. The shock location in section A-A and the wake region in section 3 have been predicted well.

The simulations showed a satisfactory prediction of the performance and flow field; hence this model was applied to other studies in this paper.

6.   RESULTS AND DISCUSSION

The results of 3-D time-dependent computations under the influence of tip injection and inlet distortion are presented in this section. Figure 9 shows the effect of the tip injection and inlet

distortion on the impeller performance. The mass flow rates are normalized against the respective choking mass flow rates at the outlet. The impeller total pressure ratio and adiabatic efficiency have been calculated based on the time-averaged and mass flow averaged parameters in sections A-A and C-C. For the injection cases, the mass flow rate at the outlet is the summation of the inlet and injected mass flow rates. The adiabatic efficiency is calculated based on Eq.(1), including the additional work done on the injected air.

$$\eta_{adb} = \frac{\left(\dfrac{P_{t_{out}}}{P_{t_{in}}}\right)^{\frac{\gamma-1}{\gamma}} - 1}{\left(\dfrac{T_{t_{out}}}{T_{t_{in}}} - 1\right) + \dfrac{m_j}{m_{out}}\left(\left(\dfrac{P_{t_j}}{P_{amb}}\right)^{\frac{\gamma-1}{\gamma}} - 1\right)} \tag{1}$$

As Fig. 9 shows, the circumferential distortion reduces the impeller total pressure ratio and adiabatic efficiency. However, it has no significant effect on the safe operating range. The near stall total pressure ratio and adiabatic efficiency are reduced by about four percent and two percentage points, respectively, due to the inlet distortion. According to this figure, using the tip injection has improved the operating range by about 30%. However, in this condition, the adiabatic efficiency is reduced to some extent (about 0.6 percent points at the design point). It can be seen that the impact rate of the tip injection on the impeller performance under clean and distorted flow conditions is approximately the same, so it can be concluded that the existence of the inlet distortion on the tip injection effectiveness is unaffected.

(a) Total pressure ratio

(b) Adiabatic efficiency
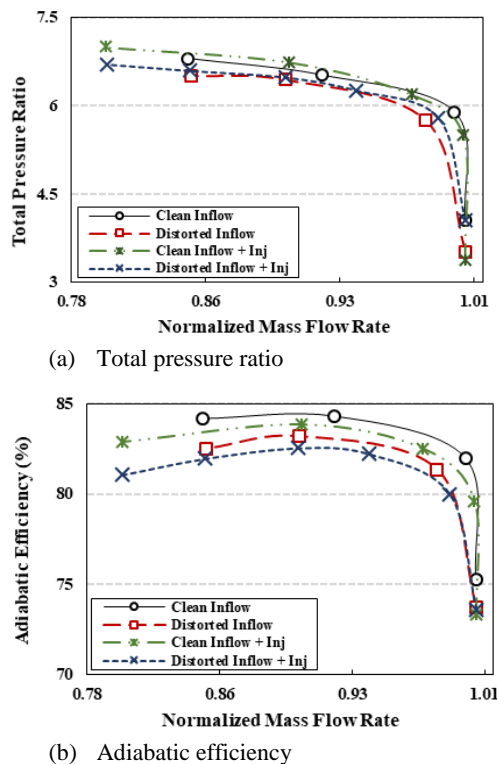
Fig. 9. The effects of the tip injection and inlet distortion on the performance curves.

The following results represent how the inlet distortion or tip injection affects the impeller flow field. All parameters are compared in the same operating condition: the normalized mass flow rate equivalent to the normalized mass flow rate for the clean inflow case with smooth casing at the near stall condition ($m_{op}/m_{choked} = 0.845$). Fig. 10 shows the circumferential distribution of the instantaneous normalized total pressure upstream of the impeller (section A-A) and at 99% span. In this figure, the total pressure is normalized with the mass flow averaged and time-averaged total pressure at the inlet of each case.
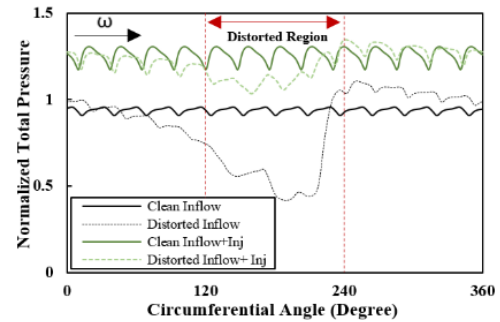
Fig. 10. Circumferential distribution of the instantaneous normalized total pressure at section A-A and 99% span.

The distortion propagation in the impeller path is observed in Fig. 10 for distorted cases. However, the interfaces of distorted and undistorted regions are no longer recognizable. As mentioned in some studies (Khaleghi and Jalaly 2016), when a compressor is exposed to circumferential inlet distortion, two swirling flows are created, one in the same direction of the blade rotation direction (co-swirl) and the other in the opposite direction of the blade motion (counter-swirl). In the co-swirl region (the entry of the distorted sector), the total pressure gradually decreases until it reaches its lowest value (counter-swirl region). Then, it increased sharply (near the distorted sector exit). This non-uniform pressure distribution may change the ability of each blade to increase pressure, which ultimately leads to a decrease in impeller performance or stability. In these conditions, loading on the blades is not uniform in the circumferential direction, which increases the flow separation and the stall occurrence possibility in some blades. This performance drop or the stability reduction can be compensated by tip injection. In addition to the total pressure increment, the tip injection has dramatically helped to even out the total pressure in the desired area, leading to increased impeller performance and flow stability. Tip injection reduces blade loading in the tip region and consequently allows the impeller stall to occur at lower mass flow rates. Similar results can be observed in the circumferential distribution of the absolute flow angle. Fig. 11 shows the circumferential distribution of the absolute flow angle at the same location and conditions applied in Fig. 10.

As shown in Fig. 11, the total pressure distortion induces flow angle non-uniformity in section A-A.
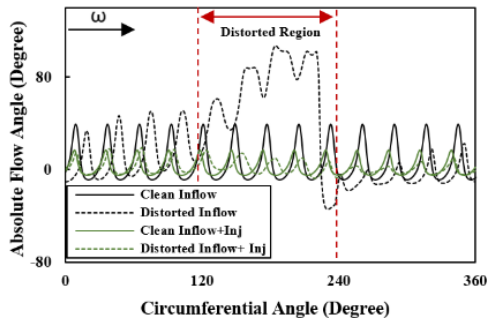
Fig. 11. Circumferential distribution of the absolute flow angle in section A-A and 99% span.

Non-uniform flow angle distribution indicates an unbalanced load distribution on the blades, which increases the probability of flow separation and the onset of instability in some blades (around $190^0 - 210^0$ circumferential position) compared to other blades. Furthermore, nearly all over the distorted sector, the flow angle in the distorted inflow case with the smooth casing is higher than in other cases. So, it can be concluded that inlet distortion can increase pressure loss or entropy production. According to this figure, the non-uniformity of the flow angle at section A-A has significantly been reduced by using the tip injection. The tip injection has reduced the flow angle in either clean or distorted inflow. In the distorted region, this effect is very noticeable. Reducing the flow angle in this area can decrease the blade loading and flow separation, leading to increased flow stability.

The static pressure contour, especially near the tip, can help to evaluate the impeller's stability. The shock wave and its interaction with tip leakage flow can be inferred from the static pressure contours. In Fig. 12, the blade-to-blade instantaneous normalized static pressure contours at 95% span in the same normalized mass flow rate ($m_{op}/m_{choked} = 0.845$) for different cases are compared (Fig. 12(a): clean inflow, (b): distorted inflow, (c): clean inflow with injection and (d): distorted inflow with injection). The static pressure is normalized with the mass flow averaged and also time-averaged total pressure at the inlet of each case. In this figure, the black arrow indicates the direction of the impeller rotation. Tip vortex projection is also specified using the black dashed line on the contours. The distorted region at the inlet is also indicated for the distorted inflow.
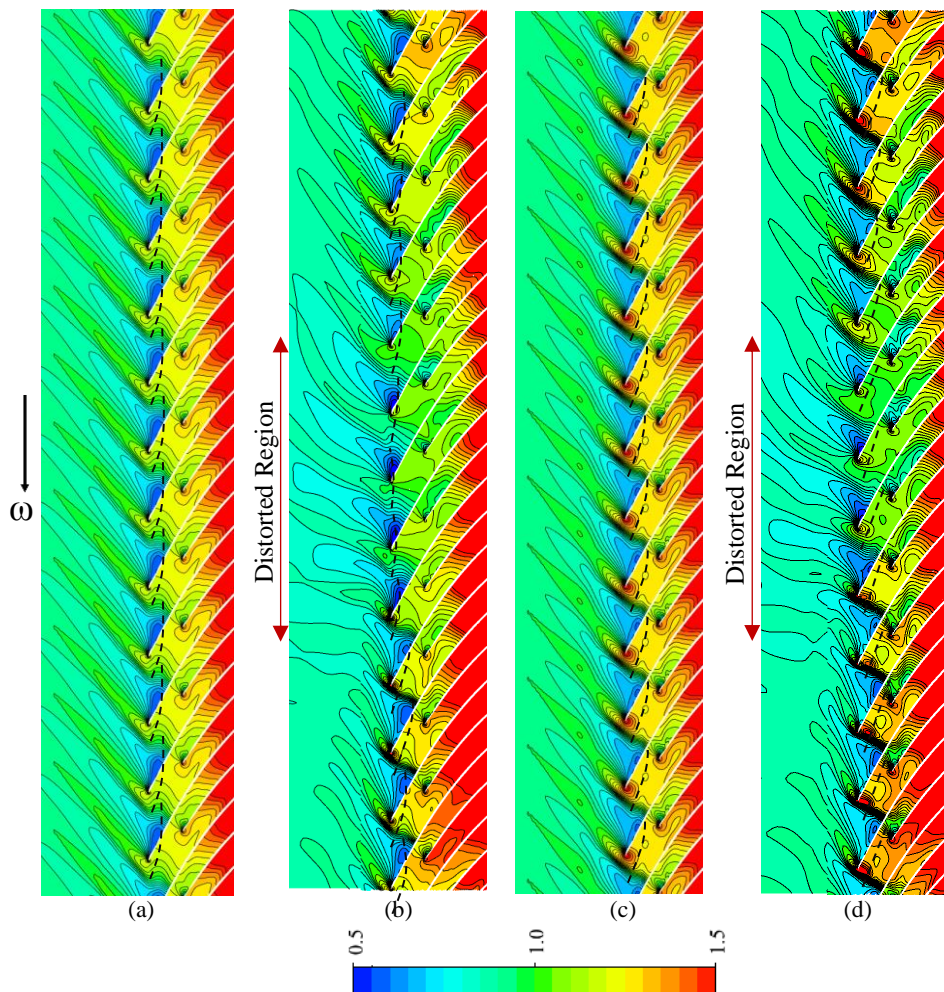
Fig. 12. Blade to blade instantaneous normalized static pressure contours at 95% span, (a) clean inflow, (b) distorted inflow, (c) clean inflow with injection, (d) distorted inflow with injection.

As shown in Fig. 12, in distorted inflow (Fig. 12(b) and (d)), when a blade passes through the distorted region, the shock structures move slightly upstream. So shock-tip leakage flow interaction in some blades gets stronger than in others. Conversely, when a blade leaves the distorted region, the shock structure moves downward, reducing the intensity of the shock-tip leakage flow interaction. In other words, some blades in distorted inflow experience higher load, which increases the probability of instability onset and flow separation in these blades.

On the other hand, the blockage caused by tip

leakage flow interaction at the impeller inlet due to upstream shock movement can be a significant cause of stall occurrence. The tip injection causes downstream shock transmission, weakening the shock-tip leakage interaction. Hence, stall inception is postponed in this condition (Fig. 12(c) and (d)).

In the flow path, many factors may cause the flow field deterioration and the impeller performance degradation, some of which can be explained by the entropy contour near the impeller tip. Fig. 13 reveals the entropy contours at the same location and the same condition applied in Fig. 12.
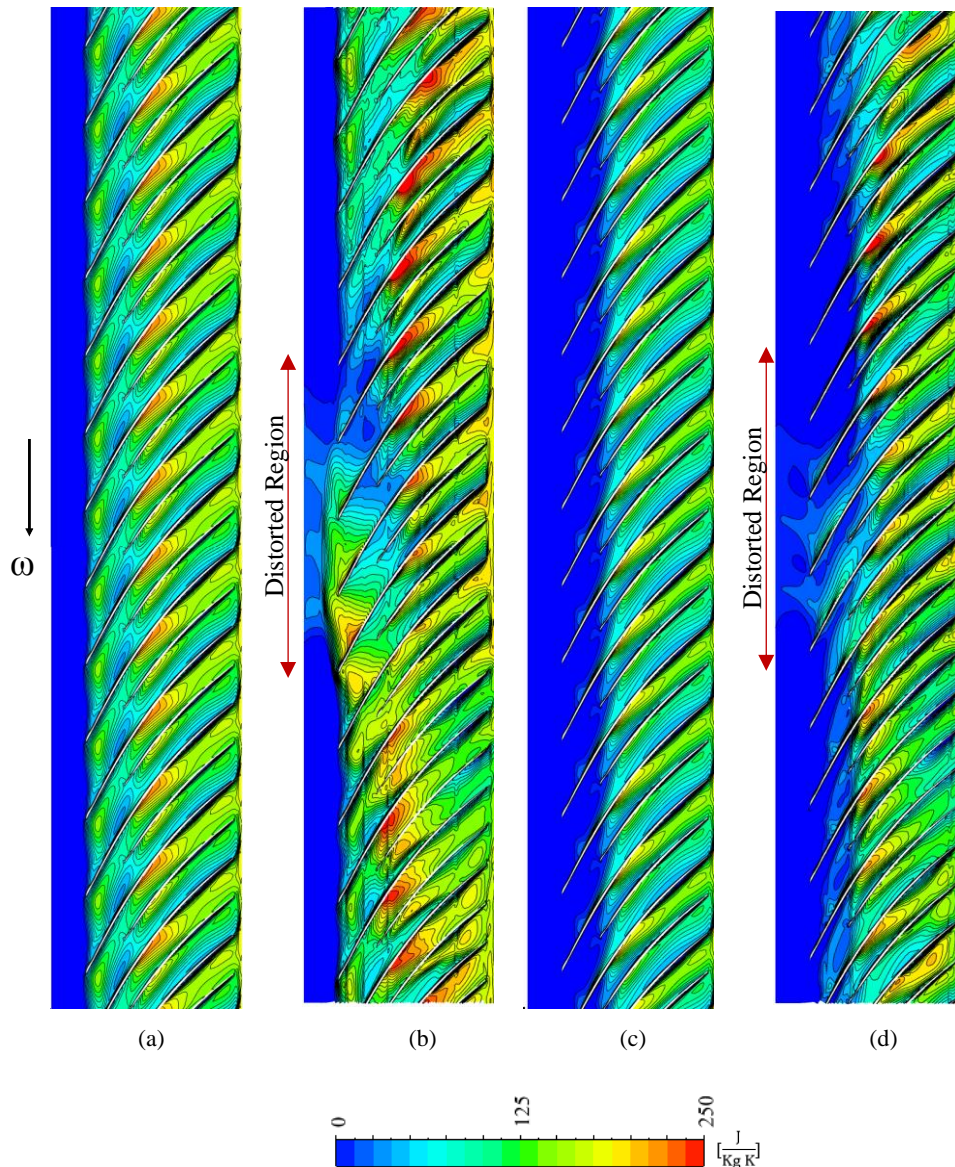
Fig. 13. Blade to blade instantaneous entropy contours at 95% span, (a) clean inflow, (b) distorted inflow, (c) clean inflow with injection, (d) distorted inflow with injection.

High entropy regions near the main blade LE are owing to shock-tip leakage flow interactions. The entropy generation from the middle of the flow path to the impeller TE is basically due to the mainstream and tip leakage flow interactions or the boundary layer separation. The high entropy zone represents more pressure loss in that region. The change in

entropy production intensity and its affected area due to inlet distortion and injection can be explained according to the contours presented in Fig. 13 According to Fig. 13(b), due to the stronger shock–tip leakage interaction in some blade passages (owing to inlet distortion), the entropy generation is
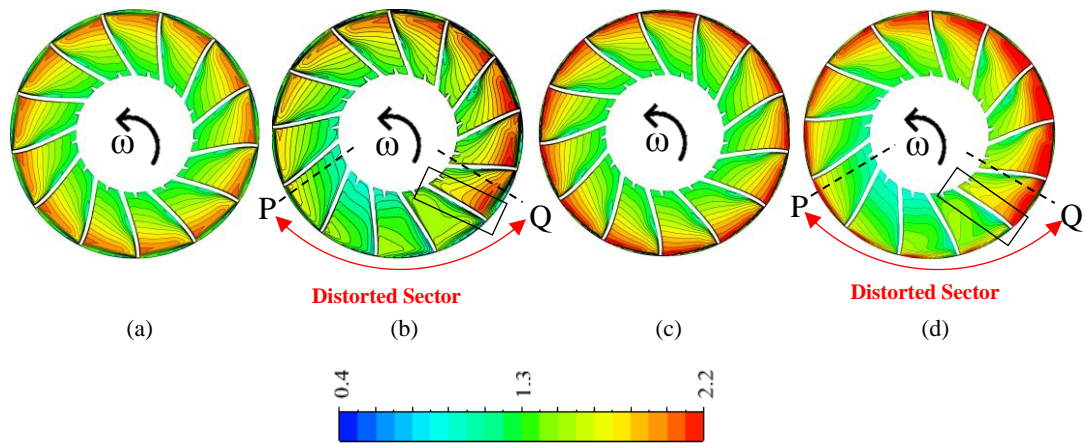
Fig. 14. Normalized instantaneous total pressure contours in the relative frame in section B-B, (a) clean inflow, (b) distorted inflow, (c) clean inflow with injection, (d) distorted inflow with injection.
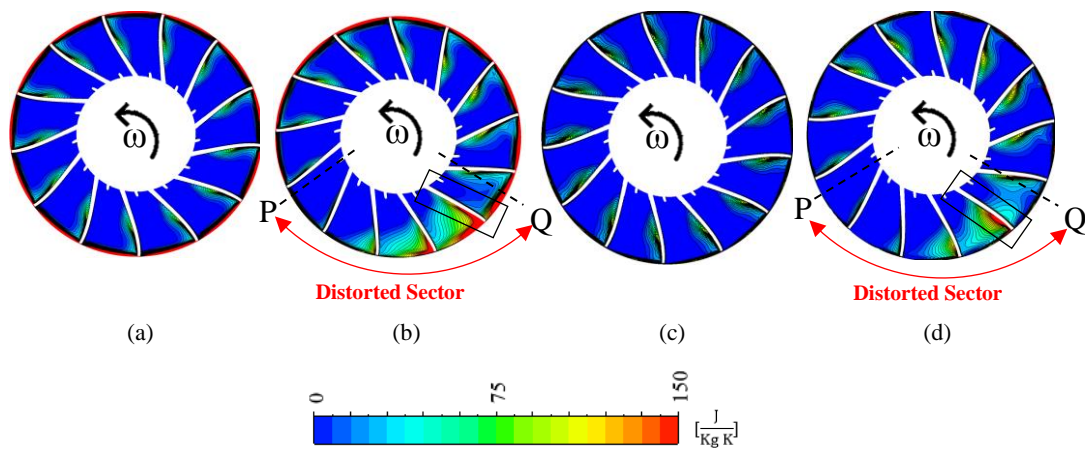
Fig. 15. Entropy contours in section B-B, (a) clean inflow, (b) distorted inflow, (c) clean inflow with injection, (d) distorted inflow with injection.

higher than in other passages, leading to higher pressure loss.

Furthermore, the entropy generation in the second half of the impeller has the highest value in the case of distorted inflow with smooth casing (Fig. 13(b)). Using the tip injection alleviates the high entropy regions by energizing the main flow near the blade tip in both clean and distorted inflow (as shown in Fig. 13(c) and 13(d)). The tip injection can reduce the tip leakage flow intensity and improve the impeller stability.

In order to study the flow changes from the root to the casing due to the inlet distortion or tip injection, the normalized instantaneous total pressure and entropy in section B-B are presented in Figs. 14 and 15 respectively. These contours are presented for different cases ((a): clean inflow, (b): distorted inflow, (c): clean inflow with injection and (d): distorted inflow with injection)) in the same normalized mass flow rate ($m_{op}/m_{choked} = 0.845$). The total pressure is normalized with the mass flow averaged and time-averaged total pressure at the inlet of each case. The direction of the impeller rotation is indicated on contours. Furthermore, sections P and Q (which are specified with black dashed lines)

correspond to the distorted and undistorted interfaces at the inlet.

The inlet distortion propagation through the impeller passage is also confirmed by the contours presented in (Fig. 14(b), Fig. 14 (d), Fig. 15(b) and Fig. 145(d)). According to Fig. 14, the total pressure is increased from the root to the casing, which occurs gradually in the clean inflow (Fig. 14(a) and Fig. 14(c)). However, in the distorted inflow (Fig. 14(b) and Fig. 14(d)) in some blade passages, the total pressure variations from the root to the casing are higher than in others. The most significant pressure difference between the pressure and suction side belongs to the blade exiting the distorted region shown with a rectangular bounding box. This blade bears the highest load compared to others, so the flow separation and entropy generation in this area will be higher than in others. The entropy contours presented in Fig. 15 confirm this conclusion, as higher entropy generation is evident in the specified area with a rectangular bounding box. According to the results of Figs. 14(c), Fig. 14(d), Fig. 15(c) and Fig. 15(d), the effect of the injection is to increase the total pressure and decrease the entropy production and loading near the blade tip, so the performance and stability improvement occurs in this condition.

The results of Figs. 14 and 15 show that although the near tip flow field is strongly affected by the inlet distortion or tip injection, the flow field near the root is not affected by inlet distortion or tip injection.

7. CONCLUSION

The full annulus numerical computations by using a URANS solver were carried out to study circumferential inlet distortion and tip injection mechanism on an impeller. The test case is an impeller of a transonic centrifugal compressor, the so-called SRV2-O. A 120-degree circumferential total pressure distortion was applied for the distorted inflow as the inlet boundary condition.

Results revealed that the inlet distortion leads to a slight decrement in the total pressure ratio and adiabatic efficiency; however, the safe operating range was not affected due to the inlet distortion. The near stall total pressure ratio and adiabatic efficiency were reduced by about four percent and two percentage points, respectively, due to the inlet distortion. The results also indicated that the tip injection has a low impact on the impeller total pressure ratio and adiabatic efficiency; however, it remarkably enhances the safe operating range. The tip injection improved the impeller operating range by approximately 30%. According to the results, the injection effectiveness is not affected by the inlet distortion. The rate of change in the performance due to tip injection in uniform or distorted inflow was approximately the same.

The flow field investigations revealed that the inlet distortion leads to the non-uniformity of other parameters such as flow angle, entropy or static pressure along the impeller path. The flow field study near the tip showed that the inlet distortion increases the pressure losses, especially those related to leakage flow; however, the tip injection considerably suppresses these high entropy zones. The tip injection improves the impeller performance and postpones the stall inception by weakening the tip leakage vortex and energizing the main flow near the tip. According to the results, although the near tip flow field is strongly affected by the inlet distortion and tip injection, the flow field near the root is not affected by them.

REFERENCES

Ariga, I., N. Kasai, S. Masuda, Y. Watanabe and I. Watanabe (1983). The effect of inlet distortion on the performance characteristics of a centrifugal compressor. *Journal of Engineering for Power* 105, 223-230.

Beheshti, B. H., K. Ghorbanian, B. Farhanieh, J. A. Teixeira and P. C. Ivey (2006). A new design for tip injection in transonic axial compressors. In *ASME turbo expo 2006: Power for land, sea, and air*, 39-47. American Society of Mechanical Engineers Digital Collection.

Dong, X., D. Sun, F. Li and X. Sun (2018) Stall margin enhancement of a novel casing treatment subjected to circumferential pressure distortion. *Aerospace Science and Technology* 73, 239-255.

Eisenlohr, G., P. Dalbert, H. Krain, H. Pröll, F. A. Richter and K. H. Rohne (1998). Analysis of the transonic flow at the inlet of a high pressure ratio centrifugal impeller. In *ASME 1998 International Gas Turbine and Aeroengine Congress and Exhibition*, V001T01A007-V001T01A007. Citeseer.

Eisenlohr, G., H. Krain, F. A. Richter and V. Tiede (2002). Investigations of the flow through a high pressure ratio centrifugal impeller. In *ASME Turbo Expo 2002: Power for Land, Sea, and Air*, 649-657. American Society of Mechanical Engineers Digital Collection.

Engeda, A., Y. Kim, R. Aungier and G. Direnzi (2003). The inlet flow structure of a centrifugal compressor stage and its influence on the compressor performance. *Journal of Fluids Engineering* 125, 779-785.

Grimaldi, A. and V. Michelassi (2019). The Impact of Inlet Distortion and Reduced Frequency on the Performance of Centrifugal Compressors. *Journal of Engineering for Gas Turbines and Power* 141, 021012.

Hah, C. and H. Krain (1999). Analysis of transonic flow fields inside a high pressure ratio centrifugal compressor at design and off design conditions. In *ASME 1999 International Gas Turbine and Aeroengine Congress and Exhibition*. American Society of Mechanical Engineers Digital Collection.

Hah, C., D. C. Rabe, T. J. Sullivan and A. R. Wadia (1998). Effects of inlet distortion on the flow field in a transonic compressor rotor. *Journal of Turbomachinery* 120, 233-246.

Hirano, T., T. Uchida and H. Tsujita (2012). Control of surge in centrifugal compressor by using a nozzle injection system: universality in optimal position of injection nozzle. *International Journal of Rotating Machinery* 2012.

Iyengar, V., L. Sankar and S. Niazi (2005). Assessment of the self-recirculating casing treatment concept applied to axial compressors. In *43rd AIAA Aerospace Sciences Meeting and Exhibit* 632.

Khaleghi, H., M. Boroomand, J. Teixeira and A. Tousi (2008a). A numerical study of the effects of injection velocity on stability improvement in high-speed compressors. *Proceedings of the Institution of Mechanical*

Engineers, Part A: Journal of Power and Energy 222**,** 189-198.

Khaleghi, H. and R. Jalaly (2016). Effects of Circumferential Inlet Distortion on the Performance of a Transonic Fan Together With the Impact of Tip Injection. In *ASME Turbo Expo 2016: Turbomachinery Technical Conference and Exposition.* American Society of Mechanical Engineers Digital Collection.

Khaleghi, H., J. A. Teixeira, A. M. Tousi and M. Boroomand (2008b). Parametric Study of Injection Angle Effects on Stability Enhancement of Transonic Axial Compressors. *Journal of Propulsion and Power* 24**,** 1100-1107.

Kim, Y., A. Engeda, R. Aungier and G. Direnzi (2001). The influence of inlet flow distortion on the performance of a centrifugal compressor and the development of an improved inlet using numerical simulations. *Proceedings of the Institution of Mechanical Engineers, Part A: Journal of Power and Energy* 215**,** 323-338.

Li, J., J. Du, S. Geng, F. Li and H. Zhang (2020). Tip air injection to extend stall margin of multi-stage axial flow compressor with inlet radial distortion. *Aerospace Science and Technology* 96**,** 105554.

Li, S., X. Yang, W. Li and M. Tang (2021). Investigating the Influence of the Inlet Bypass Recirculation System on the Compressor Performance. *Journal of Applied Fluid Mechanics* 14**,** 1295-1305.

Longley, J., H. W. Shin, R. Plumley, P. Silkowski, I. Day, E. Greitzer, C. Tan and D. Wisler (1996). Effects of rotating inlet distortion on multistage compressor stability. *Journal of Turbomachinery,* 118**,** 181-188.

Ma, S. B. and K. Y. Kim (2017). Optimization of discrete cavities in a centrifugal compressor to enhance operating stability. *Aerospace Science and Technology,* 68**,** 308-319.

Reid, C. (1969). The response of axial flow compressors to intake flow distortion. In *ASME 1969 gas turbine conference and products show*. American Society of Mechanical Engineers Digital Collection.

Spakovszky, Z., C. Van Schalkwyk, H. Weigl, J. Paduano, K. Suder and M. Bright. (1998). Rotating stall control in a high-speed stage with inlet distortion: Part II—circumferential distortion. In *ASME 1998 International Gas Turbine and Aeroengine Congress and Exhibition*, V005T15A024-V005T15A024. American Society of Mechanical Engineers.

Stein, A., S. Niazi and L. Sankar (2000). Computational analysis of stall and separation control in centrifugal compressors. *Journal of Propulsion and Power* 16**,** 65-71.

Suder, K. L., M. D. Hathaway, S. A. Thorp, A. J. Strazisar and M. B. Bright (2000). Compressor stability enhancement using discrete tip injection. *Journal of Turbomachinery* 123**,** 14-23.

Sun, Z., X. Zheng, H. Tamaki and Y. Kaneko (2019). Flow instability suppression and deep surge delay by non-axisymmetric vaned diffuser in a centrifugal compressor. *Aerospace Science and Technology* 105494.

Taghavi-Zenouz, R. and M. H. A. Behbahani (2018). Improvement of aerodynamic performance of a low speed axial compressor rotor blade row through air injection. *Aerospace Science and Technology* 72**,** 409-417.

Vagnoli, S. and T. Verstraete (2015). URANS analysis of the effect of realistic inlet distortions on the stall inception of a centrifugal compressor. *Computers & Fluids* 116**,** 192-204.

Wang, G., W. Chu, H. Zhang and Z. Guo (2021) Effect of Active Flow Control of Endwall Synthetic Jet on the Performance of a Transonic Axial Compressor. *Journal of Applied Fluid Mechanics* 14, 963–977..

Yang, Q., L. Li, Y. Zhao, J. Xiao, Y. Shu and Q. Zhang (2017). Experimental investigation of an active control casing treatment of centrifugal compressors. *Experimental Thermal and Fluid Science* 83**,** 107-117.

Zemp, A., A. Kammerer and R. S. Abhari (2010). Unsteady computational fluid dynamics investigation on inlet distortion in a centrifugal compressor. *Journal of turbomachinery* 132**,** 031015.

Zhang, M. and A. Hou (2017). Investigation on stall inception of axial compressor under inlet rotating distortion. *Proceedings of the Institution of Mechanical Engineers, Part C: Journal of Mechanical Engineering Science* 231**,** 1859-1870.

Zhang, M. and X. Zheng (2018). Criteria for the matching of inlet and outlet distortions in centrifugal compressors. *Applied Thermal Engineering* 131**,** 933-946.

Zhao, B., H. Sun, L. Wang and M. Song (2017). Impact of inlet distortion on turbocharger compressor stage performance. *Applied Thermal Engineering* 124**,** 393-402.